IEEE Access
Multidisciplinary | Rapid Review | Open Access Journal

Received September 22, 2021, accepted October 13, 2021, date of publication October 18, 2021, date of current version November 1, 2021.

Digital Object Identifier 10.1109/ACCESS.2021.3121151

Performance Analysis of Sidelink 5G-V2X Mode 2 Through an Open-Source Simulator

VITTORIO TODISCO[1,2,3], STEFANIA BARTOLETTI[1,2], (Member, IEEE), CLAUDIA CAMPOLO[2,4], (Senior Member, IEEE), ANTONELLA MOLINARO[2,4,5], (Senior Member, IEEE), ANTOINE O. BERTHET[5], (Senior Member, IEEE), AND ALESSANDRO BAZZI[2,3], (Senior Member, IEEE)

[1]CNR-IEIIT, 40136 Bologna, Italy
[2]CNIT, 43124 Parma, Italy
[3]DEI and WILAB/CNIT, Università di Bologna, 40136 Bologna, Italy
[4]DIIES, Mediterranea University of Reggio Calabria, 89122 Reggio Calabria, Italy
[5]Laboratory of Signals and Systems, CNRS, CentraleSupélec, Paris-Saclay University, 91190 Gif-sur-Yvette, France

Corresponding author: Stefania Bartoletti (stefania.bartoletti@ieiit.cnr.it)

ABSTRACT The Third Generation Partnership Project (3GPP) has recently published a new set of specifications to enable advanced driving applications in fifth generation (5G) vehicle-to-everything (V2X) scenarios, with particular effort dedicated to the sidelink resource allocation in the autonomous mode, named Mode 2. In this paper, we conduct a comprehensive analysis of Mode 2 performance via an open-source system-level simulator, which implements the 5G New Radio (NR) flexible numerology and physical layer aspects together with the newly specified sidelink resource allocation modes for V2X communications and different data traffic patterns. Results collected through extensive simulation campaigns, under a wide variety of vehicle density, data transmission settings and traffic patterns, showcase the effects of the new 5G-V2X features on the sidelink resource allocation performance and provide some insights into possible ways to further improve Mode 2 performance.

INDEX TERMS 5G-V2X, new radio, sidelink, connected vehicles, autonomous resource allocation, Mode 2, open-source simulation, LTEV2Vsim, WiLabV2Xsim.

I. INTRODUCTION

Vehicle-to-everything (V2X) communication is a key paradigm for upcoming cooperative automated driving as it enables any vehicle to communicate with other vehicles and with any other V2X-enabled entity in the vicinity for sharing their local views and intentions, discover surroundings, and coordinate driving maneuvers.

The Third Generation Partnership Project (3GPP), starting from the Releases 14 and 15 of long term evolution (LTE), has included the support of V2X within the LTE-V2X standard that proved to sustain basic V2X safety applications. More recently, the enhancements to the fifth generation (5G) system and its new radio (NR) interface have been finalized in Release 16 to accommodate advanced V2X use cases within the 5G-V2X standard, sometimes called NR-V2X. The 3GPP is currently working on further improvements of 5G-V2X in Releases 17 and 18.

Cellular V2X enables uplink and downlink communication between terminal nodes, namely user equipments (UEs), and base stations, namely gNBs, in the radio access network. Sidelink communication is also enabled and refers to the direct communication between UEs, without conveying the data through the network. Leveraging sidelink communications, vehicles, road side units (RSUs), or handheld devices carried by pedestrians, which are all considered UEs, can communicate directly with each other.

One of the key aspects in the 5G-V2X sidelink is the resource allocation, which may be either decided by the network in a controlled way or directly by the single UEs through an autonomous selection procedure. In the controlled mode, referred to as Mode 1 in 5G-V2X and Mode 3 in LTE-V2X, the base station (BS) schedules the sidelink resources attempting an ideally interference-free allocation.

The associate editor coordinating the review of this manuscript and approving it for publication was Hai Wang.

Contrarily, in the autonomous mode, referred to as Mode 2 in 5G-V2X and Mode 4 in LTE-V2X, the UEs select sidelink resources on their own by using a channel sensing mechanism which is not immune to packet collisions.

The autonomous mode is unquestionably the more challenging of the two modes as the channel sensing and distributed resource selection mechanisms play a critical role for an efficient and effective sharing of the sidelink resources among vehicles. 5G-V2X compared to LTE-V2X adds further complexity in the autonomous mode configuration and operation due its higher flexibility in both the physical (PHY) and medium access control (MAC) layer operation. First, Mode 2 relies on a PHY layer numerology which is scalable and not fixed as for Mode 4 and determines the amount of sidelink resources to be shared: the bandwidth of the resource block depends, in fact, on the subcarrier spacing, which is given by the numerology, and therefore PHY layer settings and the adopted numerology have a joint impact on the amount of available sidelink resources. Second, a more flexible MAC layer supports a larger variety of data traffic generation patterns. Indeed, unlike LTE-V2X that only supported periodic messages in its initial design, in 5G-V2X also aperiodic traffic is considered from the beginning of its specifications.

As the autonomous 5G-V2X sidelink is no longer an idea under discussion, but rather a well-defined standard [1]–[3], a thorough performance analysis that takes into account all of the above aspects is necessary to understand the effects of the main PHY and MAC layer parameters and procedures, their interplay on Mode 2 sidelink communications under a number of different scenarios and settings.

The key contributions of this paper are as follows:

- We introduce an open-source event-driven simulator, named WiLabV2Xsim, for the performance analysis of 5G-V2X. It extends LTEV2Vsim, an LTE-V2X simulator, by taking into account the flexible NR numerology and the PHY and MAC layer settings and procedures, as foreseen in 3GPP specifications [1]–[4];[1]
- We present a thorough performance analysis of 5G-V2X Mode 2 showing the impact of the new features of 5G-V2X, among which the flexible subcarrier spacing (SCS) of NR, the modulation and coding scheme (MCS) settings, the resource allocation and retransmission schemes, on the main performance metrics for V2X sidelink data exchange;
- We provide helpful guidelines for an effective parameter setting that improves the performance of Mode 2 under different vehicle densities and data traffic patterns.

The remainder of the paper is organized as follows. Section II presents the related work and details the gap that this paper is filling. Section III presents the key parameters related to the numerology and the physical layer of 5G-V2X Mode 2. Section IV introduces the Mode 2 resource allocation procedure and the main parameters taken into account within the proposed simulation framework. Section V presents the main building blocks of the implemented open-source simulator. Section VI provides simulation results with insights in the performance evaluation and hints for improvement. Finally, Section VII presents our concluding remarks.

[1]The open-source simulator WiLabV2Xsim will be freely available at https://github.com/V2Xgithub/WiLabV2Xsim. It extends LTEV2Vsim, which is an open-source simulator currently available at https://github.com/alessandrobazzi/LTEV2Vsim.

II. RELATED WORK AND PAPER SCOPE

Recently, surveys and tutorials providing a comprehensive overview of the 5G-V2X technology features have begun to follow one another, with focus on the architecture as well as the physical layer and how resources are allocated [5]–[8]. Other types of papers have started to quantitatively investigate the performance of some aspects of 5G-V2X. The work in [9] focused on the PHY layer performance of 5G-V2X, without exploring the MAC dynamics. The impact of the flexible 5G numerology on the MAC of the autonomous mode was preliminarily investigated in [10], but when considering the Mode 4 resource allocation mechanism and periodic traffic only, being this work published before the specifications of Mode 2 in Release 16. Aperiodic traffic has been recently considered in [11], where the misalignment between packet generation and resource allocation was investigated in case of Mode 4. The work in [12] extended the Mode 2 reservation scheme to specifically deal with aperiodic traffic, by inferring the probability of the packet generation intervals. In [13]–[15] the first studies on the performance of Mode 2 also appeared. In [13], the authors compare the use of Mode 2 with random allocation, providing an extensive description of the sidelink technology in 3GPP, and focusing on the effects of some key parameters used for the sensing-based resource selection. In [14], the authors mainly focus on the impact of the numerology to compare 5G-V2X Mode 2 and LTE-V2X Mode 4. In [15], the authors compare the behavior of Mode 2 in the presence of periodic and aperiodic traffic. All these studies do not elaborate on the relationship between packet size, MCS, and available resources nor analyze the key modifications introduced by the recently developed 5G-V2X Mode 2 compared to LTE-V2X Mode 4.

In this work, instead, with the aid of one of the first open-source system-level simulators on sidelink 5G-V2X, we disclose the effect of the peculiar features introduced by Mode 2 at both the PHY and MAC layers. For LTE-V2X, huge efforts have been devoted to the development of simulation platforms for the investigation of sidelink performance, with special attention to Mode 4. In most cases, the implementations are not shared publicly, hindering the reproducibility of results. However, a few solutions have also been made available as open-source, including as examples those presented in [16]–[18]. The first one [16] focuses on Mode 4 and is an extension of ns-3, based on the device-to-device (D2D) model presented in [19]. Another open-source simulator, called ms-van3t, extending ns-3 to include Mode 4 is presented in [17]. The solution presented in [18], also focusing on Mode 4, is a modification and extension of

TABLE 1. Main parameters when varying the numerology in 5G [4].

μ	$\Delta f = 2^{\mu} * 15$	Frequency Range	Cyclic Prefix	Slot duration (ms)	# Slots/Subframe	n. PRBs in 10 MHz
0	15	sub-6 GHz	Normal	1	1	52
1	30	sub-6 GHz	Normal	0.5	2	24
2	60	Any	Normal, Extended	0.25	4	11
3	120	mmWave	Normal	0.125	8	NA

the SimuLTE [20] within OMNeT++; it is implemented in two versions, one integrating with the Artery[2] framework and the second one integrating with Veins [21] only. Very recently, a few implementations of some of the 5G-V2X features have been added to ns-3 and presented in [13]–[15].

Among the open-source simulation platforms, the first appeared for the study of LTE-V2X Modes 3 and 4 was LTEV2Vsim [22]. It is written in Matlab and since its publication in 2017, it has been extensively leveraged by several research teams to evaluate the performance of Mode 4 and its extensions, e.g., in [23], and more recently in [24]–[30], just to name a few. Moreover, besides LTE-V2X, the simulator provides support for evaluating IEEE 802.11p, and it was exploited for the investigation of their co-channel coexistence in [31]–[33]. We have enhanced such platform to include 5G-V2X PHY and MAC layers, with special focus on the autonomous mode, for the performance analysis presented in this work, which complements the current literature analyzing the 5G-V2X sidelink performance.

III. 5G-V2X PHYSICAL LAYER DESIGN

5G-V2X extends LTE-V2X with the features of the 5G NR physical layer and accommodates advanced V2X applications with a broad range of requirements, thanks to the multicarrier orthogonal frequency-division multiplexing (OFDM) empowered with the versatility of the NR numerology. The design of the PHY layer for the 5G-V2X sidelink, with its flexible numerology, time-frequency resource structure, and channel organization, is briefly summarized in this Section.

A. FLEXIBLE NUMEROLOGY

3GPP specifies two large frequency ranges for NR operation, namely frequency range 1 (FR1) and frequency range 2 (FR2). The former is what is usually referred to as the sub-6 GHz band, while the latter is referred to as the millimeter wave (mmWave) band. Depending on the frequency range, the maximum channel bandwidth and the space between OFDM subcarriers (the SCS) may vary.

While in LTE the SCS was fixed as $\Delta f = 15$ kHz, 5G NR introduces the concept of flexible numerology as the value of SCS can vary, as well as the OFDM symbol duration. In particular, $\text{SCS} = 2^{\mu} * \Delta f$ and different numerologies are referenced by the parameter μ. Table 1 reports the numerologies specified by the 3GPP for the two frequency ranges [4].

Regarding the modulation, Release 16 5G-V2X supports Cyclic Prefix (CP)-OFDM not only for uplink and downlink but also for the sidelink [34]. The available subcarrier modulations are quadrature phase shift keying (QPSK), 16-quadrature amplitude modulation (QAM), 64-QAM, and 256-QAM. Different CP lengths can be associated with different SCSs in order to countermeasure different levels of inter-symbol interference (ISI) caused by the multipath fading. The NR standard gives also the possibility to use normal CP (NCP) and/or extended CP (ECP). The NCP is available for any value of SCS, whereas the ECP is possible only with SCS = 60 kHz, in both frequency ranges.

B. RESOURCE STRUCTURE

In NR, radio resources (RRs) span both time and frequency domains. In the time domain, RR are organized in frames, subframes, and slots. A frame has a 10 ms duration and is composed of 10 subframes of 1 ms duration. For sidelink transmissions, the minimum resource allocation unit in the time domain is a slot [35]. Depending on whether a normal CP or an extended CP is used, each slot consists of 14 or 12 OFDM symbols, respectively.

The slot time duration depends on the SCS and, in particular, its duration decreases as the numerology increases. For the 15 kHz SCS of LTE-V2X, the length of a slot is 1 ms, corresponding to a subframe. For higher numerologies, with 30 kHz, 60 kHz, and 120 kHz SCSs, the slot duration is 0.5 ms, 0.25 ms, and 0.125 ms, respectively. As a result, the number of slots per frame and per subframe changes according to the numerology, as indicated in Table 1. It is worth noting that larger SCSs correspond to shorter time slot duration, and so the use of higher numerologies is preferred under low-latency application requirements.

In the frequency domain, RRs are organized in resource elements (REs), physical resource blocks (PRBs), subchannels, and resource pools. Each RE is a subcarrier over an OFDM symbol, and each PRB is composed of 12 consecutive subcarriers with the same SCS. As the SCS changes, the bandwidth of a PRB varies accordingly. As a result, the number of PRBs within a fixed channel bandwidth depends on the SCS. The last column of Table 1 details the available PRBs for a given bandwidth of 10 MHz [36].

A subchannel consists of a group of M consecutive PRBs and represents the smallest allocation unit in the frequency domain for sidelink communications. M corresponds to the subchannel size, which is configured within a resource pool, and can take the following values, 10, 12, 15, 20, 25, 50, 75, or 100 PRBs [5]. A resource pool is a subset of available RRs that can be used by a group of UEs for their sidelink

[2]https://github.com/riebl/artery/

communication. A resource pool consists of contiguous PRBs and contiguous or non-contiguous slots.

In Fig. 1, the relationship between RE, subcarrier, PRB, and subchannel is provided with reference to the time and frequency domains.

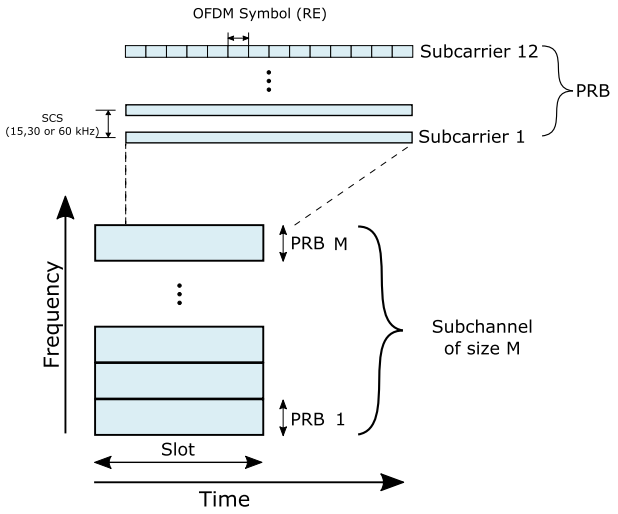

FIGURE 1. 5G-V2X time-frequency resource structure.

The number of available subchannels varies as the SCS and the PRB bandwidth vary. For example, if subchannels with a 10 PRB-size are assumed, in a given channel bandwith of 10 MHz, 5 subchannels can be accommodated for SCS = 15 kHz, 2 subchannels for SCS = 30 kHz and a single subchannel with SCS = 60 kHz.

Each transmission is performed in one time slot and one or multiple contiguous subchannels, depending on the packet size, the number of PRBs per subchannel, and the MCS. More specifically, given the packet size and MCS, the number of PRBs needed for the packet to be transmitted is determined. Lower MCS indexes correspond to a higher number of PRBs. As a consequence, there is the risk that a very low MCS index could require more PRBs than those available in a given slot for a given channel size and subchannel size. More details will be given in Section VI.

C. SIDELINK PHYSICAL CHANNELS

A sidelink physical channel is defined as a set of REs carrying user data and other control information originating from higher layers. The transmission data is organized in transport blocks (TBs), which contain the data and is associated with a sidelink control information (SCI). In 5G-V2X, each TB is associated to a SCI, which is in turn transmitted in two stages to reduce the complexity of resource sensing. The first-stage SCI is primarily used for channel sensing and is decodable by any UE. The remaining scheduling information is carried by the second-stage SCI. Then, in contrast to LTE-V2X, where only broadcast is supported, the advent of the second stage SCI in NR-V2X allows for a customizable SCI architecture that supports unicast, groupcast, and broadcast transmissions.

The transmission data, the SCI and other information are mapped onto sidelink physical channels. For sidelink communications, NR defines four sidelink physical channels:

- Physical Sidelink Shared channel (PSSCH): it conveys sidelink user data, synchronization information, control configuration data, and the 2nd stage of the SCI;
- Physical Sidelink Control Channel (PSCCH): it conveys the 1st stage of the SCI, which transports sidelink scheduling information. The information of the PSCCH must be decoded by any UE for channel sensing purposes;
- Physical Sidelink Feedback channel (PSFCH): it carries feedback related to the successful or failed reception of a sidelink transmission;
- Physical Sidelink Broadcast Channel (PSBCH): it conveys information related to synchronization and is sent periodically within a sidelink synchronization signal block, but not on slots of a resource pool.

Note that the SCI is mapped onto two distinct sidelink physical channels. The 1st stage SCI is transmitted onto the PSCCH while the 2nd stage SCI is transmitted along with its relative TB onto the PSSCH. The PSSCH can span over one or multiple subchannels according to the packet size and the adopted MCS, while the PSCCH is always located in a known position within the subchannel. The TB and its relative SCI are always transmitted in the same time slot.

D. SLOT STRUCTURE

Each data transmission, which covers in 5G-V2X one slot and one or more subchannels, starts with one symbol used for automatic gain control (AGC), which carries a copy of the second symbol. Then, in addition to the physical channels, a number of demodulation reference signals (DMRSs) is transmitted with known data to allow performing channel estimation for the correct demodulation of the physical channels. DMRSs are transmitted along each of the sidelink physical channels at configurable positions inside the slot. Different DMRS positions and time-densities can be used to cope with different scenarios (i.e., depending on the speed as this changes the dynamics of the radio channel). Higher-order numerology may require less DMRS transmissions as they are associated with shorter slot duration. The position of the DMRS inside the slot is referenced in the SCI. An empty guard symbol concludes the slot to allow transmission to reception switch and time adjustments.

The 3GPP specifications permit high variability in the configuration and Fig. 2 shows two examples, where the PSCCH entirely occupies the used subchannel for three symbols and two symbols are dedicated to the DMRSs.

E. RETRANSMISSIONS

Sidelink retransmissions can be used to improve the communication reliability for 5G-V2X use cases with stringent requirements. In Mode 2, this can be done either through blind retransmissions or through HARQ-feedback. In the blind retransmission, a pre-configured number of

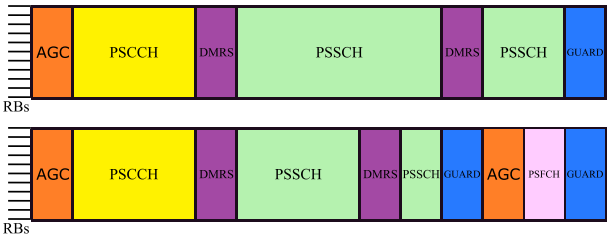

FIGURE 2. Examples of 5G-V2X slot structure without (top) and with (bottom) feedback channel. In the examples, the control channel consists of three symbols and two symbols are dedicated to the DMRS.

retransmissions can be performed for each message without any feedback; blind retransmissions allow to increase the probability of correct reception not only because more attempts are performed to decode the message, but also because the signals received can be combined at the receiver and increase the overall signal-to-interference-plus-noise ratio (SINR). In the presence of HARQ-feedback, the transmission over the PSFCH is performed by a receiving UE as response to a transmission over the PSSCH previously received. For broadcast transmissions, only blind retransmissions are supported, while HARQ-feedback is also available for groupcast and unicast communications.

IV. AUTONOMOUS RESOURCE ALLOCATION IN 5G-V2X

In Release 16, the 3GPP re-defines the scheduling of resources with additional features and mechanisms. In this section, the scheduling of resources for the LTE-V2X Mode 4 (i.e., before Release 16) and the 5G-V2X Mode 2 (i.e., from Release 16 on) are presented.

A. LTE-V2X MODE 4

In Mode 4, UEs autonomously select the resources for their transmission using the sensing-based semi-persistent scheduling (SB-SPS) specified in Release 14 under the assumption of periodic traffic. The procedure for the selection of resources consists of two phases: *(i)* channel sensing and *(ii)* resource selection. During the channel sensing phase, the UE senses the radio channel and detects ongoing transmissions by decoding the SCIs transmitted by other users. Together with SCI decoding, the UE measures also the reference signal received power (RSRP) and calculates its average value over a sensing window of 1 s preceding the slot at which new resources must be selected. The average is done to include all transmissions that were performed in the past and that correspond to a periodicity that can conflict with the allocation that is being performed.

To identify a suitable resource for the transmission, the UE starts from all the possible allocations excluding those for which it lacks information (for example because it was not able to sense the medium due to half duplexing) and then builds a shorter list of candidate resources from which the selection can occur. This list of resources, namely L2, consists of a percentage M of the resources that have been least interfered and therefore, are less prone to collisions. By default, M is equal to 20%. The UE then randomly selects a resource from the L2 list. The resource corresponding to the same subchannels is then periodically reserved every resource reservation interval (RRI), which is a time interval assumed equal to the packet generation periodicity and constrained to some specific values (i.e., 20 ms, 50 ms, or any multiple of 100 ms up to 1 s). The number of transmitting periods before the resource is reevaluated is equal to the reselection counter, which is a discrete number initialized randomly, e.g., between 5 and 15 if RRI $\geq$100 ms. When the reselection counter reaches zero, the resource is changed with probability $1 - p_k$ (p_k is set by the operator between 0 and 0.8); with probability p_k, instead, the resource is kept for another random interval. The only alternative to the periodic allocation described above can be done by setting the RRI to 0, which means that there are no subsequent reservations.

B. 5G-V2X MODE 2

In Mode 2, analogously to Mode 4, the UEs autonomously select the sidelink resources for their transmission, without the support from the network. In addition to the SB-SPS, 5G-V2X explicitly introduces the dynamic scheme for the allocation and scheduling of aperiodic traffic. With the dynamic scheme, the selected resource is only used for one transmission, and resources can be reserved for its own retransmission only. Therefore, with the dynamic scheme, at each transmission, new resources must be selected. The resource selection procedure is the same for both the semi-persistent and dynamic scheme and it involves, like in Mode 4, the sensing and resource selection phase. The sensing window in the 5G-V2X Mode 2 case can have a duration of either 1100 ms or 100 ms according to the configuration that is set for each resource pool. During this period of time, the UE senses and decodes the SCIs sent by other UEs on the sidelink channel. The decoded SCIs are stored together with the measurement of the RSRP and this information is used to determine which resources must be excluded when a new resource selection is required. In Mode 2, resources can be excluded from being possible candidate resources if and only if the associated information is not available (e.g., measurements were not performed because the station was transmitting) or they are reserved by a prior SCI with an associated RSRP above a given threshold. After the exclusion process, a resource is selected randomly from the set of the remaining available resources. Analogously to LTE-V2X Mode 4, also in 5G-V2X Mode 2, when the SB-SPS is used, the resource is used for a number of consecutive periods according to the reselection counter, with the same rules defined for Mode 4. The time period between the selected resources for consecutive transmission is determined by the RRI reported in the SCI, which can be selected in 5G-V2X in a larger set of values (i.e., any integer number of milliseconds between 1 and 99 ms or any multiple of 100 ms up to 1 s). Blind retransmissions, if present, are also advertised in the

SCI. Each SCI can reserve up to two retransmissions, with full flexibility in frequency and time in a window of 32 slots.

Figure 3 schematizes the resource allocation of Mode 2. During the sensing period, the sensing UE becomes aware of the neighboring transmitting UEs. The sensed aperiodic and periodic transmissions are represented in yellow and red, respectively. The difference between the two is that periodic transmissions reserve the same resource after a period equal to the selected RRI. Transmissions can occupy one or more adjacent subchannels. A past transmission of the sensing UE is represented in violet. No sensing information is available during the time at which UEs transmit, due to the half-duplex limitations. Lastly, the remaining available resources after the exclusion process are represented in orange.

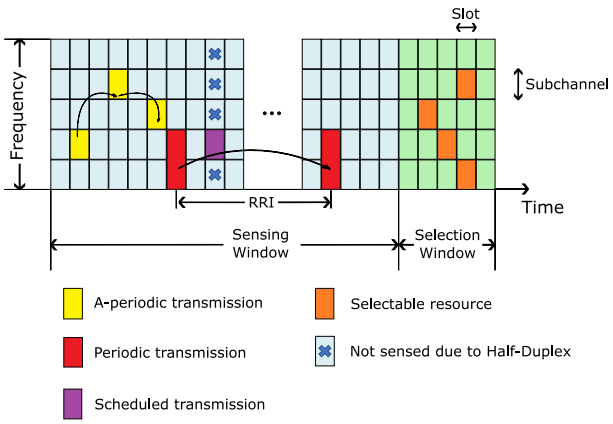

FIGURE 3. Mode 2 resource allocation scheme.

It is important to highlight that the described Mode 2 re-engineers Mode 4. In particular,

1) The averaging operation of the RSRP measurements over the sensing window is removed (only the value corresponding to the TB directly associated to the SCI is used);
2) The L2 list is not built nor considered.

The removal of the averaging operation for the RSRP measurements has two main effects. On the one hand, a positive effect is that without the averaging operation, the more recent measurements are more important than the less recent ones, which might be related to obsolete reservations; this is particularly true in highly dynamic environments. On the other hand, without the averaging operation, there could be possible issues if the last reservation has been lost, which might occur even with exactly periodic traffic. In such a case, the system is in fact not able to detect the busy status of a resource.

The removal of the L2 list instead implies that partly and possibly highly interfered resources are passed to the higher layers for selection, contrarily to Mode 4 that uses the L2 list and therefore selects the resources among the least interfered ones.

The drawbacks of the average and L2 removal appear clear in the case where the SB-SPS is enforced but the generation of the packets does not perfectly correspond to the periodic resource allocation, which we call *incoherent traffic generation*, as opposed to a perfect correspondence, called *coherent traffic generation*. Fig. 4 shows an example of coherent and incoherent traffic generation. In Fig. 4, a resource is selected for being used over time with a given RRI and either 1) the packet generation period is coherent with the RRI (top of the figure) or 2) the packet generation is not coherent with the RRI (bottom of the figure). In the incoherent case, which assumes in the example one new packet every two RRIs, due to the absence of the averaging operation of the RSRP and of the L2 list, the resource is considered empty after the time instants b and d, with higher probability of collisions on resources c and e.

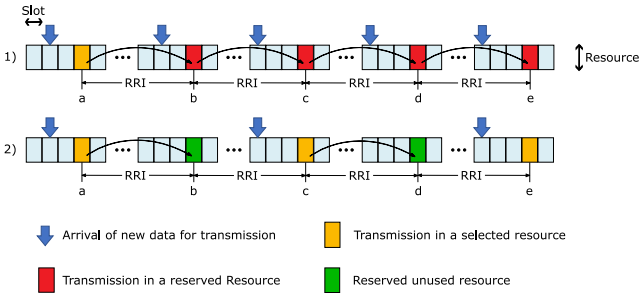

FIGURE 4. Coherent (top) and incoherent (bottom) packet generation, with respect to the RRI.

V. THE OPEN-SOURCE SIMULATOR IN BRIEF

The open-source discrete event simulator LTEV2Vsim was designed for the investigation of resource allocation techniques for V2V connectivity, with focus mainly on sidelink LTE-V2X, through the support for both Mode 3 and Mode 4. Later improved with the support of IEEE 802.11p, it is here extended and renamed as WiLabV2Xsim to include the new features of Mode 2 of 5G-V2X, including also the NR numerology and the proper PHY layer settings. All relevant parts of the protocol stack are accurately reproduced, with a realistic generation of the messages at the facilities layer, a careful implementation of the MAC level protocol, a detailed definition of the radio resources at the PHY layer based on the various settings (e.g., numerology, channel bandwidth, subchannel size, MCS, packet size, etc.) and the modeling of packet reception as hereafter detailed.

Fig. 5 shows a concise block diagram of the simulator in its use for the investigation of 5G-V2X. The first step is the initialization procedure, which sets the starting position of the vehicles, the available physical radio resources (including the available subchannels), and an initial assignment of resources. The position of the vehicles can be taken either from a given theoretical model or from realistic traffic traces. For the former approach, both highway and Manhattan grid scenarios are implemented, in alignment with [37].

Once the simulation is started, the simulator processes one after the other the occurring events: position update, packet

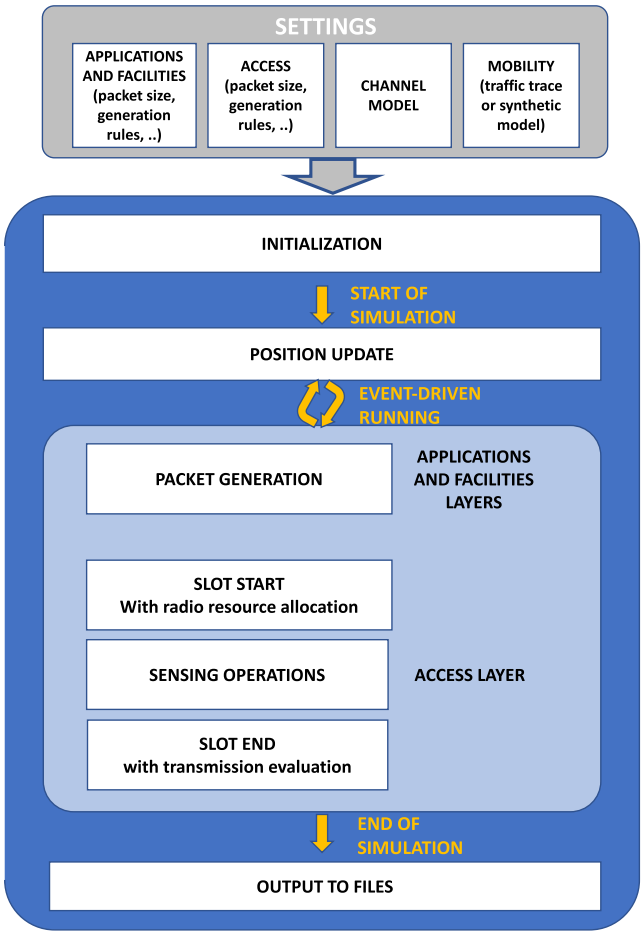

FIGURE 5. Block scheme of WiLabV2Xsim when running 5G-V2X.

generation, and slot-start/slot-end. More specifically, at regular intervals vehicle positions are updated, which implies an update of path-loss and large-scale fading (shadowing) values. Asynchronously from the position update, packets are generated following the statistics of interest. Also asynchronously with respect to the previous events, the slots are finally processed, with actions taken at their beginning and end, where the end of the slot corresponds to the last instant before the time gap used as guard interval (see Section III). Before the slot-starts, new resource allocations are performed if needed. Then, the nodes that reserved a resource and have a packet waiting in the queue, start their transmission; all the other vehicles act as possible receivers. At the slot-end, the correctness of the transmissions is evaluated, with an update of the output metrics and an update of the measurements used for the SB-SPS procedure.

The core part of the evaluation consists in detecting whether each transmission succeeded or not. Denoting the transmitting vehicle as i, the receiving vehicle as j, and the slot under consideration as t, the average SINR is obtained as

$$\gamma_{ij,t} = \frac{h_{ij,t} P_{\mathrm{t}i} / L(d_{ij})}{P_{\mathrm{n}} + I_{ij,t}}, \tag{1}$$

where $P_{\mathrm{t}i}$ is the power transmitted by i, $h_{ij,t}$ is the large-scale fading contribution to the link from i to j in slot t, $L(d_{ij})$ is the path-loss from i to j as a function of the distance from i to j, P_{n} is the noise power, and $I_{ij,t}$ is the average interference. In (1), the numerator represents the useful received power, whereas the denominator is the sum of the noise power and the interference, assumed Gaussian with zero mean. $I_{ij,t}$ is in turn defined as:

$$I_{ij,t} = \sum_{k \in \mathcal{V}_t, k \neq i} \eta_{ki} \frac{h_{kj,t} P_{\mathrm{t}k}}{L(d_{kj})}, \tag{2}$$

where $\mathcal{V}_t$ is the set of the nodes transmitting in slot t, and η_{ki} is a multiplying coefficient, between 0 and 1, that quantifies how much power is sent by k in the subchannels used by i, related to the transmission power of k. η_{ki} is 1 if k uses exactly the same subchannels as i, and is lower than 1 if its signal does not overlap or it overlaps only partially. The calculation of η_{ki} takes into account the in-band emission (IBE) in alignment with the specifications in [36].

When blind retransmissions are considered, if the first transmission fails, the corresponding average SINR is saved and summed to the average SINR of the second transmission, thus implementing maximal ratio combing (MRC).

Once the average SINR is calculated, either it can be used to assess statistically the outcome of the transmission using link-level curves detailing packet error rate (PER) vs. SINR, or it can be compared with a SINR threshold (calculated as detailed in Appendix A) to assess whether the transmission is successful or not. The small-scale fading is implicitly included in the curves or threshold. Whereas the former approach is slightly more accurate, the latter allows to simulate any combination of packet sizes and MCS indices without the need of storing a large number of link-level curves and to avoid resorting to interpolation subroutines.

Based on the outcome of each transmission, the simulator provides output performance metrics, including, among others, packet reception ratio (PRR), end-to-end delay (EED), and packet inter-reception (PIR).

VI. PERFORMANCE EVALUATION

In this section, simulation settings and metrics are first described and then the results achieved through the implemented open-source simulator are analyzed focusing on Mode 2. First, the effect of the numerology, MCS and retransmissions is investigated, followed by an insight into the impact of two key modifications to the resource allocation process, i.e., the L2 list removal and the new calculation of the received power within the sensing window.

A. SIMULATION SETTINGS AND METRICS

In this subsection, the settings of the simulations are detailed in terms of evaluation scenario, channel modeling, and data traffic model. A summary of the main settings is also provided in Table 2.

TABLE 2. Main simulation parameters and settings. (*) Values used if not differently specified.

Scenario	
Road layout	Highway, 3+3 lanes
Density	100 vehicles/km (*)
Average speed	70 km/h
Power and propagation	
Channels	ITS bands at 5.9 GHz
Bandwidth	10 MHz
Transmission power density	13 dBm/MHz
Antenna gain (tx and rx)	3 dBi
Noise figure	9 dB
Propagation model	WINNER+, Scenario B1
Shadowing	Variance 3 dB, decorr. dist. 25 m
Data traffic	
Packet generation	Every 100 ms (*)
Packet size	350 bytes
Physical layer (5G-V2X)	
MCS	4 (QPSK, $R_c = 0.3$) (*)
SINR threshold	Derived as in Appendix A
Subchannel size	10 PRBs
Number of subchannels	5 (*)
Access layer (5G-V2X)	
Retransmissions	Disabled (*)
Keep probability	0.4
RSRP sensing threshold	-126 dBm (*)
Min. time for the allocation, T_1	1 ms
Max. time for the allocation, T_2	100 ms

1) EVALUATION SCENARIO

We consider a Highway scenario with road configuration parameters aligned to [37]: a 2 km-long straight highway with 3 lanes per direction and wrap-around (i.e., a vehicle exiting on one side of the scenario, enters from the other side in the same lane). Each vehicle moves at a speed that is a Gaussian random variable with 70 km/h average and 7 km/h standard deviation. Unless differently specified, we assume a density of 100 vehicles/km.

2) POWER SETTINGS AND CHANNEL MODEL

The UEs transmit within the 5.9 GHz band in a 10 MHz channel bandwidth with a constant spectral power density of 13 dBm/MHz. They have an antenna gain equal to 3 dBi at both the transmitter and receiver sides. The noise figure of the receiver is assumed equal to 9 dB.

The path-loss model follows the WINNER+, scenario B1, with correlated log-normally distributed shadowing, characterized by a standard deviation of 3 dB and a decorrelation distance of 25 m, as in [38]. Given the highway scenario, line-of-sight (LOS) conditions are assumed.

The correct reception of each packet is detected as discussed in Section V, based on a SINR threshold obtained as detailed in Appendix A. The RSRP threshold is set to -126 dBm when not differently specified.

3) DATA TRAFFIC MODEL AND LINK LEVEL SETTINGS

Without loss of generality, packets of 350 bytes [39] are hereafter considered when not differently specified, either periodically generated every 100 ms or with a variable generation interval. As an example, but with the aim to adopt a realistic synthetic model, when a variable packet generation interval is adopted we derive such interval from the rules for the generation of cooperative awareness messages (CAMs), like in [11]. Some of the results have been collected also assuming larger packets to model the information-rich nature of advanced services; in particular, we have considered packet size of 1000 bytes with a 100 ms generation interval, resembling the worst case generation pattern of collective perception messages (CPMs) [40] in a highway scenario, according to [41].

At the access layer, subchannels of 10 PRBs are assumed, corresponding to current regulations in Europe for LTE [42]. The number of subchannels in the 10 MHz bandwidth depends on the numerology and corresponds to 5 subchannels with $\mu = 0$ (SCS $= 15$ kHz), which is used hereafter when not otherwise stated. Unless differently indicated in the text, MCS 4 is used, which corresponds to QPSK modulation, coding rate $R_c = 0.3$; under these settings, all 5 subchannels are required to accommodate a 350 bytes-long packet.

4) PERFORMANCE METRICS

We evaluate the performance in terms of PRR, which is derived as the average ratio between the number of neighbours correctly decoding a message at a given distance and the total number of neighbours at the same distance. It corresponds to PRR type 1 in [37].

Additionally, we measure the *range*, defined as the maximum distance from the transmitter at which the PRR remains above a certain value, say 0.9 [43].

B. IMPACT OF NUMEROLOGY AND MCS

In the first simulation campaign, the performance of different numerologies (SCS=15, 30, 60 kHz, see Table 1) and MCSs is evaluated. The effect of retransmissions is also investigated, by considering a single blind retransmission.

Before getting into the simulation results, an insight into the resources that follow different MCS and SCS settings is provided. To this aim, the number of orthogonal resources available in one 10 MHz channel and in a period of 10 frames (i.e., 100 ms) is shown for packets of 350 bytes (Fig. 6(a)) or 1000 bytes (Fig. 6(b)), when varying the MCS and SCS.[3]

It can be observed from Fig. 6 that SCS $= 30$ kHz and SCS $= 60$ kHz can only be used after a certain MCS index. For example, SCS $= 30$ kHz requires an MCS equal to or larger than 11 with 350 byte packets and 22 with 1000 byte packets; if SCS $= 60$ kHz is adopted, at least MCS 19 is needed with 350 byte packets, whereas none of the available MCSs allow to carry a 1000 byte packet. With a lower MCS, the available frequency resources are in fact not enough to accommodate a packet in a single slot. As a consequence, if lower MCSs are needed to improve robustness, such as in the case of V2X broadcast communications, then a lower

[3]In the example, the maximum number of non-overlapping (therefore orthogonal) resources are shown. However, transmissions that partially overlap in the frequency domain, i.e., that use the same subchannels for part of the allocation, are possible and indeed allowed in the simulator.

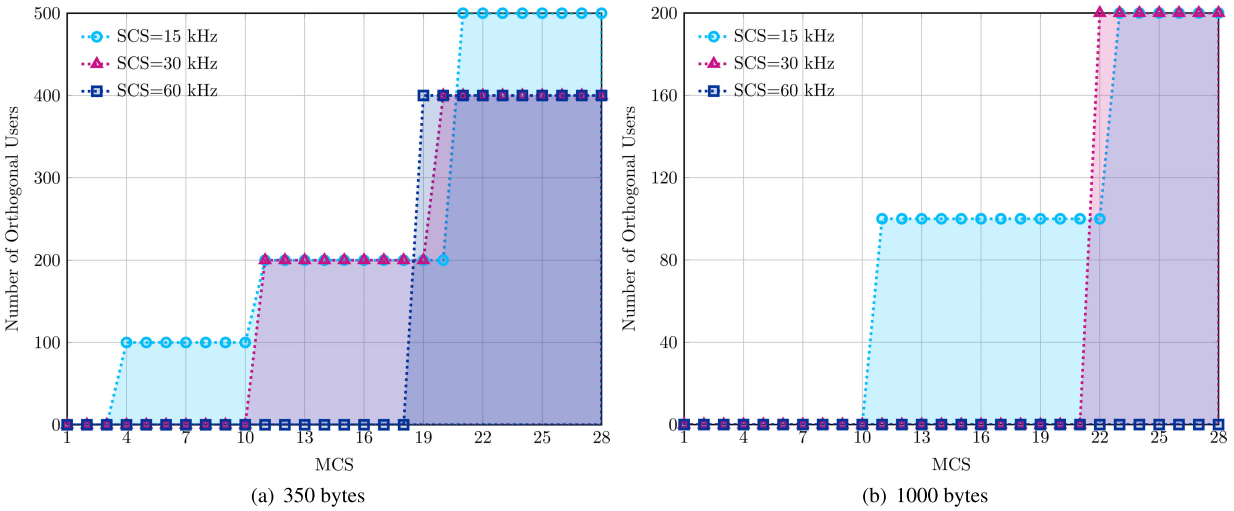

FIGURE 6. Number of available resources over a 100ms-long time window when varying the MCS index, assuming 10 MHz channel, subchannels of 10 PRBs and (a) packets of 350 bytes or (b) packets of 1000 bytes, for different numerology settings.

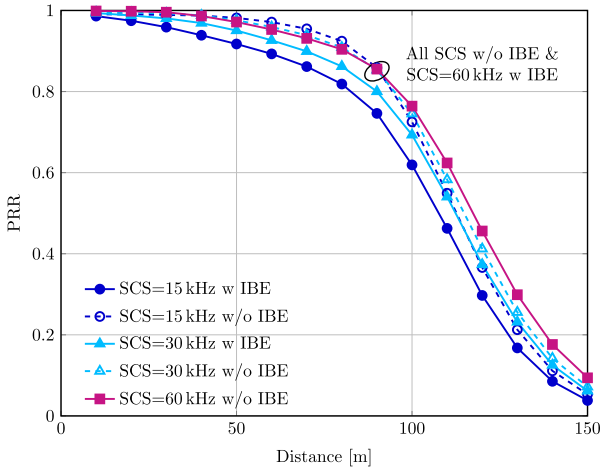

FIGURE 7. PRR for different 5G SCS configurations and MCS=21, without retransmissions, both when considering and neglecting IBE.

SCS must be adopted or a larger channel bandwidth must be selected. If both the channel bandwidth and the MCS cannot be increased, then higher order SCS might be relegated to the transmission of small packets only.

Fig. 7 shows the PRR as a function of the distance from the transmitter. For the sake of a fair comparison with different SCS settings, MCS = 21 is used; it is the lowest MCS where a similar number of orthogonal users can be allocated assuming 350 byte packets, as derived from Fig. 6(a). With MCS = 21 each packet of 350 bytes occupies 10 PRBs, which can be allocated using 1 subchannel. Note that when SCS = 15 kHz, there are 5 subchannels available in each slot; hence, up to 5 orthogonal transmissions from different UEs can be allocated on the same slot.[4] For SCS = 30 kHz and SCS = 60 kHz the possible orthogonal allocation resources per slot are reduced to 2 and 1, respectively. So the interference between different UEs using different resources but on the same slot, namely the IBE, is significantly reduced for SCS = 30 kHz and completely removed for SCS = 60 kHz. The reduction of the IBE implies a significant performance improvement, as observable in Fig. 7 and in agreement with what noted in [10]. To corroborate this statement, we also provide in Fig. 7 the results by neglecting IBE for the cases with SCS = 15 kHz and SCS = 30 kHz; as it can be observed, when the IBE is not considered the results for different SCS are comparable. It is however to note that, as observed discussing Fig. 6, the advantage of having a higher SCS and thus a lower IBE is constrained by the number of subchannels available for the given bandwidth and SCS, which might be insufficient for a reliable transmission (i.e., adopting a low MCS) of large packets.

Fig. 8 shows the range when varying the MCS and the density of vehicles, both with or without blind retransmissions. As the MCS increases, on the one side each packet occupies a decreasing number of subchannels, which means that the number of resources available for selection increases (see Fig. 6) and therefore potentially the average interference decreases; on the other side, the SINR required for correctly decoding the packet increases, possibly reducing the reliability of the communication. Overall, under the considered settings it can be observed that the best configuration for the PRR is the one with the lowest MCS as it shows the highest robustness. Furthermore, the figure confirms that adding a retransmission increases congestion and it is a favorable choice only when a small portion of the resources is used, i.e., only when the vehicle density is relatively low with a small MCS (i.e., 50 v/km), or when a high MCS is used. At higher vehicle densities, when low MCS settings (i.e., 4) are considered, retransmissions cause an increase in congestion which generally leads the performance to get worse.

[4] In the absence of IBE.

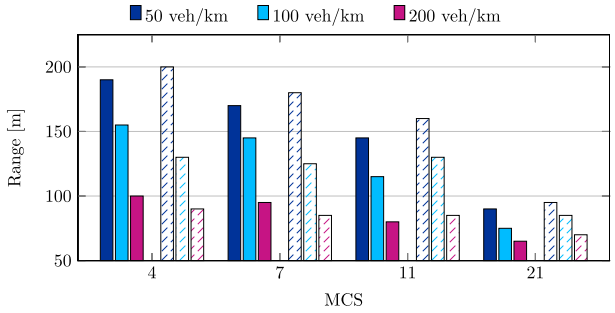

FIGURE 8. Range when varying the traffic density (SCS=15 kHz), without retransmission (solid) and with blind retransmission (dashed).

Without loss of generality, in the following we consider MCS = 4 as it showed the best performance in Fig. 8. Since blind retransmissions are shown to be effective only under a lightly loaded scenario, they are disabled in the rest of the simulations.

C. IMPACT OF THE L2 LIST REMOVAL

As a further study, we evaluate the effects of the L2 list removal for packet size equal to 350 and 1000 bytes. For 1000 byte packets an MCS equal to 11 is considered, which lets a packet occupy the same number of resources as a 350 byte packet sent with MCS equal to 4 (i.e., 5 sub-channels). In Fig. 9, the PRR performance of the Legacy Mode 2, i.e., without the L2 list, is compared to the case where the L2 list is adopted. In the latter case, different percentages of least interfered resources used as candidate ones are considered, i.e., $M = 20\%$ (corresponding to what used in LTE-V2X Mode 4) or $M = 50\%$. Results are also reported for two values of the RSRP sensing threshold: -110 and -126 dBm, where the former corresponds to the value commonly used in studies dealing with LTE-V2X Mode 4 (e.g., [44], [45]), and the latter is the minimum possible value.

As observable, the curves have similar trends in the two subfigures, with a lower range when 1000 bytes are assumed due to the less reliable MCS.

The figure shows that when the threshold is set to -110 dBm, the case with the L2 list and $M = 20\%$, outperforms both the case with $M = 50\%$ and the case without the L2 list (intuitively corresponding to $M = 100\%$). The reason is that by increasing M, more resources that are already used by other vehicles in the neighborhood are considered as available, thus causing a higher probability of collisions. Differently, when the threshold is reduced to -126 dBm, all the curves are comparable and the effect of the L2 list is negligible, for any M settings and for both packet size settings. Indeed, in this case it is more likely that the resources indicated as busy by the SCI have also an associated power exceeding the sensing threshold.

To further showcase the impact of the L2 list and of the threshold setting, results in terms of the range metric are reported in Fig. 10. For example focusing on 350 byte packets (Fig. 10(a)), it can be observed that when the L2 list is removed and the threshold is set to -110 dBm, the range metric is 110 m, compared to the 170 m that can be reached with the adoption of the L2 list. When the threshold is decreased, the effect of the L2 list removal is mitigated. Indeed, with a -126 dBm threshold, the performance with and without the L2 list is comparable.

The results shown in Figs. 9 and 10 reveal that the removal of the L2 list in 5G-V2X Mode 2 makes the RSRP threshold become a critical parameter, which needs to be kept small in order to avoid the (blind) selection of interfering resources that are already in use. This is different from LTE-V2X, where the value of the RSRP threshold has a minor impact on the performance [45]–[47].

D. IMPACT OF AVERAGING IN THE SENSING PROCEDURE

The last simulation campaign is aimed to evaluate the effects of the removal of the averaging step from the sensing procedure. As described in Section IV and through example 2 of Fig. 4, this is particularly relevant in the case of incoherent traffic generation, which is a possible situation when realistic traffic is assumed.

More specifically, instead of a constant and uniform generation of the packets, here the messages are generated following the ETSI rules for CAM messages [48]. This means that CAMs are generated based on the vehicle changes of position or speed. As a consequence, each vehicle will have messages generated periodically, but with a period that changes from vehicle to vehicle. The average generation period is approximately 207 ms [11]. Under these conditions, it was demonstrated in [11] that assuming an RRI of 100 ms and leaving empty some of the reserved resources was a good approach for LTE-V2X Mode 4. Therefore, a similar approach is here evaluated for 5G-V2X Mode 2.

In Fig. 11, the PRR when varying the distance is shown for a number of different configurations. In particular, the following cases are compared assuming the incoherent traffic generation: *(i)* the legacy Mode 2; *(ii)* Mode 2, with the L2 list with $M = 20\%$ and performing the average of the RSRP over the last 1 s (to resemble the behaviour of Mode 4); *(iii)* Mode 2, performing the average of the RSRP over the last 1 s; *(iv)* Mode 2, with the L2 list with $M = 20\%$. As an additional benchmark, it is also shown what happens with the legacy Mode 2 if coherent traffic generation is assumed; in order to have a similar data traffic pattern, 200 ms for both generation period and RRI is assumed in such case.

It can be observed in Fig. 11, that the performance of Mode 2 worsens significantly when incoherent traffic generation is assumed compared to the case in which generation period and RRI are aligned. This is because a UE would wrongly detect the reserved but unused resource over the last (100 ms-long) sensing window as free. Interestingly, it can be noted that a relevant improvement can only be achieved by reintroducing both the average of the RSRP and the L2 list. In that case, and only in that case, the performance in fact approximates the one achieved under coherent

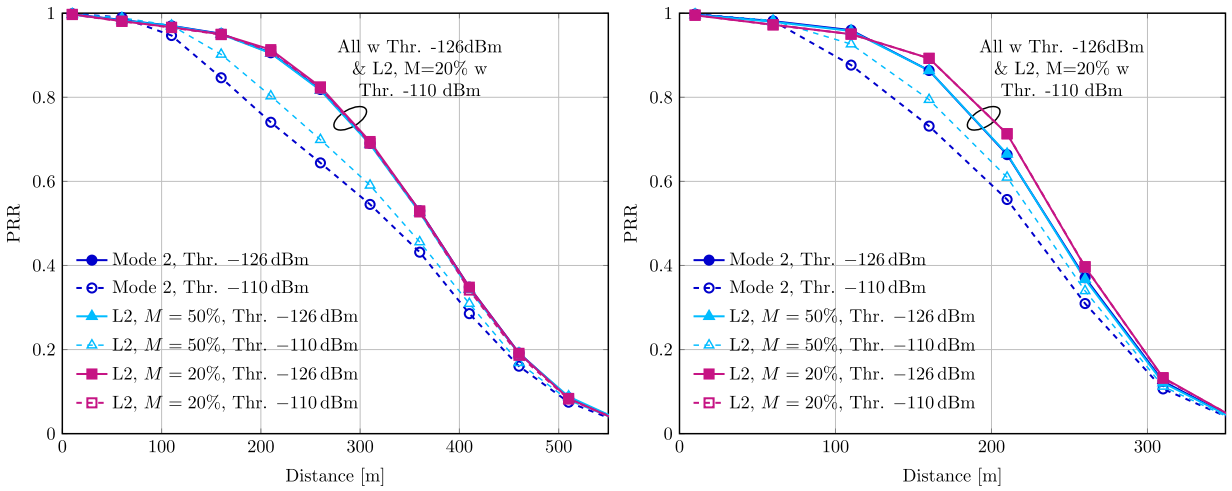

(a) 350 bytes (b) 1000 bytes

FIGURE 9. PRR in the presence or absence of the L2 list, for different *M* settings, when decreasing the RSRP sensing threshold (Thr.) from −110 dBm (dashed) to −126 dBm (solid) (SCS=15 kHz). The cases with −126 dBm are overlapping, together with the case L2, *M* = 20%, Thr. −110 dBm.

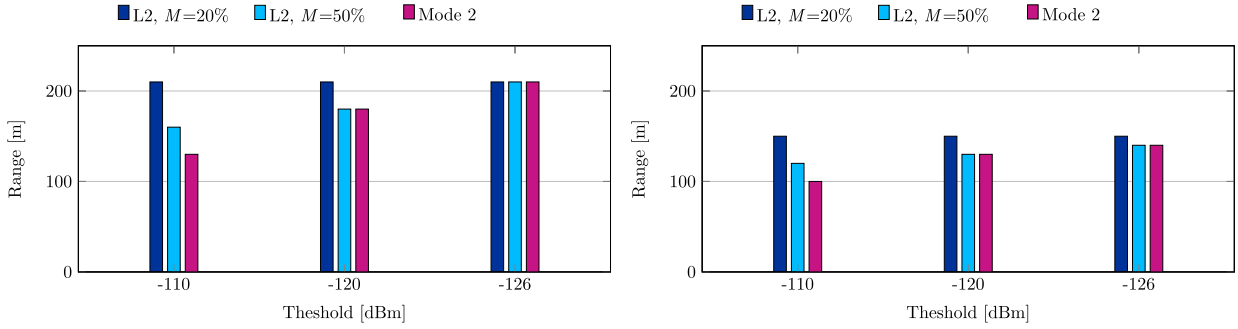

(a) 350 bytes (b) 1000 bytes

FIGURE 10. Range with and without the L2 list, when varying the RSRP sensing threshold, for different *M* settings (SCS=15 kHz).

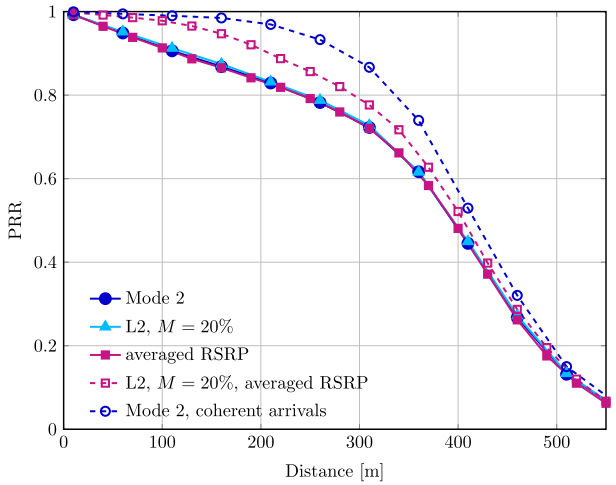

FIGURE 11. PRR for coherent and incoherent arrivals when varying the allocation scheme and the averaging process.

traffic generation. Indeed, considering a longer sensing window over which RSRP values are averaged and selecting the resource among those actually detected as less interfered provides a less myopic allocation under variable packet generation. Differently, when even only one of the two mechanisms is removed, then the scheduling is no longer able to detect future resources occupations and a lower PRR is observed, confirming the strict interplay among the two mechanisms as conceived in Mode 4.

All in all, these results show that having removed the averaging step and the L2 list, reserving resources for periodic allocations without using them could have a worse impact on performance of 5G-V2X Mode 2 compared to LTE-V2X Mode 4.

VII. CONCLUSION

In this paper, we analyzed the performance of sidelink Mode 2 with special focus on the novel features introduced in 5G-V2X compared to the previous 3GPP releases, i.e., the flexible NR numerology and modifications to the resource selection mechanism encompassing different procedures and settings for the sensing and the identification of the candidate resources. Results have been achieved through a properly overhauled open-source system-level simulator under a wide range of vehicle density, MCS, and data traffic pattern settings.

The study provides a set of helpful guidelines for understanding how the newly added features to the autonomous mode by 5G-V2X affect the reliability performance of packets exchanged over the sidelink. The effects have been measured for each feature both individually and jointly with others, while also disclosing the impact of other crucial settings.

With reference to physical layer features, in order to leverage large SCSs, which provide PRR improvements, either a higher channel bandwidth should be available or high MCS settings. However, benefits of a large SCS can be still achieved for smaller packets even with a lower MCS, which has been proven to ensure a higher robustness.

Furthermore, blind retransmissions are shown to be especially effective at low densities, otherwise they risk to further increase the load on the channel. This confirms the need for enforcing more sophisticated load-aware retransmission policies.

Interesting insights about the most appropriate setting of the RSRP sensing threshold are also provided to make the best of the Mode 2 resource selection mechanism. This tuning is specifically needed because Mode 2 does not distinguish the level of interference of resources detected as occupied over the recent past.

All the above findings apply to strictly periodic traffic. The study also focused on realistic (variable) packet generation patterns. It was proved that the persistent reservation regardless of the actual packet generation interval, with potential unused resources, which was previously shown to be quite effective in Mode 4, is instead surprisingly ineffective in Mode 2. In such a case, either a new resource selection per each message or an RRI setting which is more in agreement with the traffic generation needs to be performed by the UE.

APPENDIX

In this Appendix, the calculation of the SINR threshold used to assess the correctness of each transmission is provided, which depends on the adopted MCS m and packet size B (in bytes). Given m and B, we derive: 1) the modulation order, with the corresponding number of bits per symbol $b_{\text{symbol}}(m)$ from [35, Table 5.1.3.1-1]; and 2) the transport block size $b_{\text{TBS}}(m, B)$, in bits, according to the procedure described in [35, Clause 8.1.3.2]; for the sake of precision, it can be noted that the calculation of $b_{\text{TBS}}(m, B)$ is also influenced by the configuration of the physical channels (e.g., the number of the DMRS symbols). With the obtained values, the actual coding rate R_{c} can be calculated as:

$$R_{\text{c}} = \frac{b_{\text{TBS}}(m, B)}{n_{\text{RE}} \cdot b_{\text{symbol}}(m)}, \tag{3}$$

where n_{RE} is the number of REs dedicated to the transmission of the PSSCH except those used for the second stage of the SCI. Consequently, the number of data bits per second per Hz carried by the given MCS, denoted by $b_{\text{Hz}}(m, B)$, can be calculated as:

$$b_{\text{Hz}}(m, B) = \frac{n_{\text{sypslot}} \cdot n_{\text{scpPRB}} \cdot b_{\text{symbol}}(m) \cdot R_{\text{c}}}{t_{\text{slot}}\, f_{\text{PRB}}}, \tag{4}$$

where n_{sypslot} is the number of sidelink symbols present in a slot, which is always 14, n_{scpPRB} is the number of subcarriers in the frequency domain per PRB, which is always 12, and t_{slot} and f_{PRB} are the duration of the slot and the bandwidth of a PRB, respectively, which depend on the numerology (although their product is always 180).

By inverting the Shannon's normalized capacity formula for the Gaussian channel with a parametric factor loss Φ, which accounts for non-Gaussian signaling, finite-length coding, imperfect decoding process and other protocol's overheads, the SINR threshold can be obtained as:

$$\gamma^*(m, B) = 2^{\frac{b_{\text{Hz}}(m,B)}{1-\Phi}} - 1. \tag{5}$$

The factor loss Φ is here set to 0.6 following the recommendations of [49]. As examples, γ^* is reported for $B = 350$ and $B = 1000$ bytes in Table 3, together with N_{PRB} which is the number of PRBs required to transmit a packet of a given size, with a given MCS.

TABLE 3. Number of required PRBs N_{PRB} and minimum SINR threshold γ^* for different packet sizes and MCSs, with SCS 15 kHz; Q_{m} indicates the modulation order (number of bits per RE).

MCS	*Qm*	*350 bytes*		*1000 bytes*	
		N_{PRB}	γ^*	N_{PRB}	γ^*
0	2	107	-3.34	292	-3.35
1	2	82	-1.87	224	-1.92
2	2	68	-0.76	183	-0.76
3	2	53	0.82	141	0.85
4	2	44	2.11	116	2.15
5	2	36	3.65	95	3.61
6	2	31	4.93	81	4.89
7	2	27	6.23	69	6.31
8	2	24	7.87	61	7.51
9	2	22	8.90	54	8.81
10	4	22	8.89	54	8.81
11	4	20	10.13	49	9.95
12	4	18	11.64	43	11.63
13	4	16	13.59	39	13.25
14	4	15	15.43	35	15.00
15	4	14	16.87	32	16.60
16	4	13	17.83	30	17.87
17	6	13	17.83	30	17.87
18	6	12	19.05	28	19.02
19	6	11	21.47	26	21.02
20	6	11	23.30	24	23.04
21	6	10	25.57	22	25.08
22	6	10	27.78	21	27.76
23	6	9	29.86	20	29.40
24	6	9	32.42	18	31.78
25	6	9	33.65	18	33.31
26	6	8	35.79	17	35.69
27	6	8	37.33	16	37.27
28	6	8	38.90	16	38.44

REFERENCES

[1] *Overall Description of Radio Access Network (RAN) Aspects for Vehicle-to-Everything (V2X) Based on LTE and NR; Release 16*, 3GPP, document TR 37.895 v16.0.0, Jul. 2020.

[2] *Technical Specification Group Radio Access Network; NR; Physical Layer Procedures for Control; Release 16*, 3GPP, document TS 38.213 V16.4.0, Dec. 2020.
[3] *technical Specification Group Radio Access Network; NR; Medium Access Control (MAC) Protocol Specification; Release 16*, 3GPP, document TS 38.321 V16.3.0, Dec. 2020.
[4] *Technical Specification Group Radio Access Network; Evolved Universal Terrestrial Radio Access (E-UTRA); User Equipment (UE) Radio Transmission and Reception*, 3GPP, document TS 38.101 V16.4.0, Jun. 2020.
[5] M. H. C. Garcia, A. Molina-Galan, M. Boban, J. Gozalvez, B. Coll-Perales, T. Sahin, and A. Kousaridas, "A tutorial on 5G NR V2X communications," *IEEE Commun. Surveys Tuts.*, vol. 23, no. 3, pp. 1972–2026, 3rd Quart., 2021.
[6] S.-Y. Lien, D.-J. Deng, C.-C. Lin, H.-L. Tsai, T. Chen, C. Guo, and S.-M. Cheng, "3GPP NR sidelink transmissions toward 5G V2X," *IEEE Access*, vol. 8, pp. 35368–35382, 2020.
[7] S. A. Ashraf, R. Blasco, H. Do, G. Fodor, C. Zhang, and W. Sun, "Supporting vehicle-to-everything services by 5G new radio release-16 systems," *IEEE Commun. Standards Mag.*, vol. 4, no. 1, pp. 26–32, Mar. 2020.
[8] K. Ganesan, J. Lohr, P. B. Mallick, A. Kunz, and R. Kuchibhotla, "NR sidelink design overview for advanced V2X service," *IEEE Internet Things Mag.*, vol. 3, no. 1, pp. 26–30, Mar. 2020.
[9] W. Anwar, N. Franchi, and G. Fettweis, "Physical layer evaluation of V2X communications technologies: 5G NR-V2X, LTE-V2X, IEEE 802.11bd, and IEEE 802.11p," in *Proc. IEEE 90th Veh. Technol. Conf. (VTC-Fall)*, Sep. 2019, pp. 1–7.
[10] C. Campolo, A. Molinaro, F. Romeo, A. Bazzi, and A. O. Berthet, "5G NR V2X: On the impact of a flexible numerology on the autonomous sidelink mode," in *Proc. IEEE 2nd 5G World Forum (5GWF)*, Sep. 2019, pp. 102–107.
[11] S. Bartoletti, B. M. Masini, V. Martinez, I. Sarris, and A. Bazzi, "Impact of the generation interval on the performance of sidelink C-V2X autonomous mode," *IEEE Access*, vol. 9, pp. 35121–35135, 2021.
[12] Y. Yoon and H. Kim, "A stochastic reservation scheme for aperiodic traffic in NR V2X communication," in *Proc. IEEE Wireless Commun. Netw. Conf. (WCNC)*, Mar. 2021, pp. 1–6.
[13] Z. Ali, S. Lagen, L. Giupponi, and R. Rouil, "3GPP NR V2X mode 2: Overview, models and system-level evaluation," *IEEE Access*, vol. 9, pp. 89554–89579, 2021.
[14] M. M. Saad, M. T. R. Khan, S. H. A. Shah, and D. Kim, "Advancements in vehicular communication technologies: C-V2X and NR-V2X comparison," *IEEE Commun. Mag.*, vol. 59, no. 8, pp. 107–113, Aug. 2021.
[15] L. Lusvarghi and M. L. Merani, "MoReV2X—A new radio vehicular communication module for Ns-3," in *Proc. IEEE 94th Veh. Technol. Conf. (VTC-Fall)*, Oct. 2021, doi: 10.36227/techrxiv.16577621.v1.
[16] F. Eckermann, M. Kahlert, and C. Wietfeld, "Performance analysis of C-V2X mode 4 communication introducing an open-source C-V2X simulator," in *Proc. IEEE 90th Veh. Technol. Conf. (VTC-Fall)*, Sep. 2019, pp. 1–5.
[17] M. Malinverno, F. Raviglione, C. Casetti, C.-F. Chiasserini, J. Mangues-Bafalluy, and M. Requena-Esteso, "A multi-stack simulation framework for vehicular applications testing," in *Proc. 10th ACM Symp. Design Anal. Intell. Veh. Netw. Appl.*, Nov. 2020, pp. 17–24.
[18] B. McCarthy and A. O'Driscoll, "OpenCV2X mode 4: A simulation extension for cellular vehicular communication networks," in *Proc. IEEE 24th Int. Workshop Comput. Aided Modeling Design Commun. Links Netw. (CAMAD)*, Sep. 2019, pp. 1–6.
[19] R. Rouil, F. J. Cintrón, A. Ben Mosbah, and S. Gamboa, "Implementation and validation of an LTE D2D model for Ns-3," in *Proc. Workshop Ns-3 (WNS3)*, 2017, pp. 55–62.
[20] A. Virdis, G. Stea, and G. Nardini, "Simulating LTE/LTE-advanced networks with SimuLTE," in *Simulation and Modeling Methodologies, Technologies and Applications*, M. S. Obaidat, T. Ören, J. Kacprzyk, and J. Filipe, Eds. Cham, Switzerland: Springer, 2015, pp. 83–105.
[21] C. Sommer, R. German, and F. Dressler, "Bidirectionally coupled network and road traffic simulation for improved IVC analysis," *IEEE Trans. Mobile Comput.*, vol. 10, no. 1, pp. 3–15, Jan. 2010.
[22] G. Cecchini, A. Bazzi, B. M. Masini, and A. Zanella, "LTEV2 Vsim: An LTE-V2 V simulator for the investigation of resource allocation for cooperative awareness," in *Proc. 5th IEEE Int. Conf. Models Technol. Intell. Transp. Syst. (MT-ITS)*, Jun. 2017, pp. 80–85.
[23] B. Kang, S. Jung, and S. Bahk, "Sensing-based power adaptation for cellular V2X mode 4," in *Proc. IEEE Int. Symp. Dyn. Spectr. Access Netw. (DySPAN)*, Oct. 2018, pp. 1–4.
[24] J. Choi and H. Kim, "A QoS-aware congestion control scheme for C-V2X safety communications," in *Proc. IEEE Veh. Netw. Conf.*, Dec. 2020, pp. 1–8.
[25] Y. Yoon and H. Kim, "An evasive scheduling enhancement against packet dropping attacks in C-V2X communication," *IEEE Commun. Lett.*, vol. 25, no. 2, pp. 392–396, Feb. 2021.
[26] Y. Yoon and H. Kim, "Balancing power and rate control for improved congestion control in cellular V2X communication environments," *IEEE Access*, vol. 8, pp. 105071–105081, 2020.
[27] S. Sharma and B. Singh, "Context aware autonomous resource selection and Q-learning based power control strategy for enhanced cooperative awareness in LTE-V2 V communication," *Wireless Netw.*, vol. 26, no. 6, pp. 4045–4060, Aug. 2020.
[28] B. Kang, J. Yang, J. Paek, and S. Bahk, "ATOMIC: Adaptive transmission power and message interval control for C-V2X mode 4," *IEEE Access*, vol. 9, pp. 12309–12321, 2021.
[29] J. M. Yang, H. Yoon, S. Hwang, and S. Bahk, "PRESS: Predictive assessment of resource usage for C-V2 V mode 4," in *Proc. IEEE Wireless Commun. Netw. Conf. (WCNC)*, Mar. 2021, pp. 1–6.
[30] K. Sehla, T. M. T. Nguyen, G. Pujolle, and P. B. Velloso, "A new clustering-based radio resource allocation scheme for C-V2X," in *Proc. Wireless Days (WD)*, Jun. 2021, pp. 1–8.
[31] K. Z. Ghafoor, M. Guizani, L. Kong, H. S. Maghdid, and K. F. Jasim, "Enabling efficient coexistence of DSRC and C-V2X in vehicular networks," *IEEE Wireless Commun.*, vol. 27, no. 2, pp. 134–140, Apr. 2020.
[32] A. Bazzi, A. Zanella, I. Sarris, and V. Martinez, "Co-channel coexistence: Let ITS-G5 and sidelink C-V2X make peace," in *IEEE MTT-S Int. Microw. Symp. Dig.*, Nov. 2020, pp. 1–4.
[33] "White paper on ITS-G5 and sidelink LTE-V2X co-channel coexistence mitigation methods," CAR 2 CAR Communication Consortium, Tech. Rep. 2091, Version: 1.0, 2021. Accessed: Apr. 27, 2021. [Online]. Available: http://chrome-extension://efaidnbmnnnibpcajpcglclefindmkaj/viewer.html?pdfurl=https%3A%2F%2Fwww.car-2-car.org%2Ffileadmin%2Fdocuments%2FGeneral_Documents%2FC2CCC_WP_2091_Co-ChannelCoexistence_MitigationMethods_V1.0.pdf&clen=5426505&chunk=true
[34] *Study on NR Vehicle-to-Everything (V2X); Release 16*, 3GPP, document TR 38.885 v16.0.0, Mar. 2019.
[35] *Technical Specification Group Radio Access Network; Evolved Universal Terrestrial Radio Access (E-UTRA); Physical Layer Procedures for Data*, 3GPP, document TS 38.214 V16.2.0, Jun. 2020.
[36] *Technical Specification Group Radio Access Network; NR; User Equipment (UE) Radio Transmission and Reception; Part 1: Range 1 Standalone*, 3GPP, document T 38.101 v17.1.0, Mar. 2021.
[37] *Study on Evaluation Methodology of New Vehicle-to-Everything (V2X) Use Cases for LTE and NR; Release 15*, 3GPP, documen t TR 37.885 v15.3.0, Jun. 2019.
[38] *Technical Specification Group Radio Access Network; Study on LTE-Based V2X Services*, 3GPP, document TR 36.885 v16.2.0, Jul. 2019.
[39] V. Martinez and F. Berens, "Survey on ITS-G5 CAM statistics," 3GPP, CAR 2 CAR Commun. Consortium, Tech. Rep., TR2052, Dec. 2018.
[40] *Intelligent Transport System (ITS); Vehicular Communications; Basic Set of Applications; Analysis of the Collective Perception Service (CPS); Release 2*, document ETSI TR 103 562 V2.1.1, 2019.
[41] *Position Paper on Road Safety and Road Efficiency Spectrum Needs in the 5.9 GHz for C-ITS and Cooperative Automated Driving*, C2C-CC, 2020. Accessed: Oct. 27, 2017. [Online]. Available: http://chrome-extension://efaidnbmnnnibpcajpcglclefindmkaj/viewer.html?pdfurl=https%3A%2F%2Fwww.car-2-car.org%2Ffileadmin%2Fdocuments%2FGeneral_Documents%2FC2C-CC_Position_Paper_LTE-V2X_Oct_2017_TR_2047.pdf&clen=2082578&chunk=true
[42] *Intelligent Transport Systems (ITS); Access Layer Specification for Intelligent Transport Systems Using LTE Vehicle to Everything Communication in the 5, 9 GHz Frequency Band*, document ETSI TS 103 613 v1.1.1, 2018.
[43] H. Seo, K.-D. Lee, S. Yasukawa, Y. Peng, and P. Sartori, "LTE evolution for vehicle-to-everything services," *IEEE Commun. Mag.*, vol. 54, no. 6, pp. 22–28, Jun. 2016.
[44] R. Molina-Masegosa and J. Gozalvez, "LTE-V for sidelink 5G V2X vehicular communications: A new 5G technology for short-range vehicle-to-everything communications," *IEEE Veh. Technol. Mag.*, vol. 12, no. 4, pp. 30–39, Dec. 2017.
[45] A. Bazzi, G. Cecchini, A. Zanella, and B. M. Masini, "Study of the impact of PHY and MAC parameters in 3GPP C-V2V mode 4," *IEEE Access*, vol. 6, pp. 71685–71698, 2018.

[46] L. F. Abanto-Leon, A. Koppelaar, and S. H. de Groot, "Subchannel allocation for vehicle-to-vehicle broadcast communications in mode-3," in *Proc. IEEE Wireless Commun. Netw. Conf. (WCNC)*, Apr. 2018, pp. 1–6.

[47] R. Molina-Masegosa, J. Gozalvez, and M. Sepulcre, "Configuration of the C-V2X mode 4 sidelink PC5 interface for vehicular communication," in *Proc. 14th Int. Conf. Mobile Ad-Hoc Sensor Netw. (MSN)*, Dec. 2018, pp. 43–48.

[48] *Intelligent Transport Systems (ITS); Vehicular Communications; Basic Set of Applications; Part 2: Specification of Cooperative Awareness Basic Service*, 3GPP, document EN 302.637-2 v1.3.1, Sep. 2014.

[49] *Technical Specification Group Radio Access Network; Evolved Universal Terrestrial Radio Access (E-UTRA); Radio Frequency (RF) System Scenarios*, 3GPP, document TR 36.942 V13.0.0, Jan. 2016.

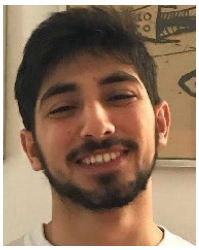

VITTORIO TODISCO received the Laurea degree in telecommunications engineering from the University of Bologna, Italy, in 2020. He is currently an Assistant Researcher with the Institute of Electronics, Computer and Telecommunication Engineering (IEIIT), National Research Council of Italy (CNR) and CNIT/WILAB.

STEFANIA BARTOLETTI (Member, IEEE) received the Laurea degree *(summa cum laude)* in electronics and telecommunications engineering and the Ph.D. degree in information engineering from the University of Ferrara, Italy, in 2011 and 2015, respectively.

From 2016 to 2019, she was a Marie Skłodowska-Curie Global Fellow within the H2020 European Framework for a research project with the Massachusetts Institute of Technology and the University of Ferrara. She is currently a Researcher with the Institute of Electronics, Computer and Telecommunication Engineering (IEIIT), National Research Council of Italy (CNR), and an Associate Member of CNIT/WILAB. Her research interests include theory and experimentation of wireless networks for localization and vehicular communications.

Dr. Bartoletti was a recipient of the 2016 Paul Baran Young Scholar Award of the Marconi Society. From 2017 to 2020, she served as a Chair of the TPC for the IEEE International Conference on Communications Workshop on Advances in Network Localization and Navigation (ANLN). She is also an Editor of the IEEE COMMUNICATIONS LETTERS.

CLAUDIA CAMPOLO (Senior Member, IEEE) (Senior Member, IEEE) received the Laurea degree in telecommunications engineering and the Ph.D. degree from the Mediterranea University of Reggio Calabria, Italy, in 2007 and 2011, respectively. She was a Visiting Ph.D. Student with the Politecnico di Torino, in 2008, and a DAAD Fellow with the University of Paderborn, Germany, in 2015. Since March 2020, she has been an Associate Professor of telecommunications with the Mediterranea University of Reggio Calabria. Her main research interests include vehicular networking, 5G and beyond systems, and future internet architectures. She is a member of the editorial board of several international journals and the Co-Editor of the book *Vehicular Ad Hoc Network: Standards, Solutions and Research* (Springer-Verlag, 2015). She has received three best paper awards for research in the vehicular networking field and the IEEE ComSoc EMEA Outstanding Young Researcher Award in 2015. She gave tutorials on V2X topics at IEEE WCNC 2012, 2018 and 2019, IEEE ICC 2017, EuCNC 2017, and IEEE PIMRC 2019. She was invited to participate to the Dagsthul Seminar on "Inter-vehicular Communication Towards Cooperative Driving," May 2018. She is a Guest Editor of several special issues on vehicular networking topics: *Computer Communications* (2016), *Future Internet* journal (2019), and the IEEE OPEN JOURNAL ON INTELLIGENT TRANSPORTATION SYSTEMS (2021).

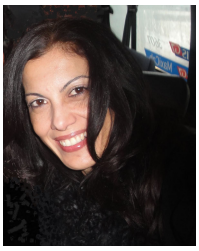

ANTONELLA MOLINARO (Senior Member, IEEE) graduated in computer engineering from the University of Calabria, in 1991. She received the Master's Diploma degree in information technology from the CEFRIEL/Polytechnic of Milano, in 1992, and the Ph.D. degree in multimedia technologies and communications systems, in 1996. She is currently an Associate Professor of telecommunications with the Mediterranea University of Reggio Calabria, Italy. She is also a Professor with the CentraleSupélec, Université Paris-Saclay, France. Before, she was with the University of Messina (1998–2001) and the University of Calabria (2001–2004) as an Assistant Professor; with the Polytechnic of Milano as a Research Fellow (1997–1998); and with Siemens A.G., Munich, Germany as a CEC Fellow in the RACE-II Program (1994–1995). Her current research interests include 5G, vehicular networking, and future internet architectures.

ANTOINE O. BERTHET (Senior Member, IEEE) received the Engineer's degree from Télécom SudParis, Evry, France, in 1997, the M.Sc. degree in signal processing from Télécom ParisTech, France, in 1997, the Ph.D. degree in computer science, electronics, and telecommunications from the University Pierre et Marie Curie (UPMC), Paris, France, in 2001, the Ph.D. degree in computer science from Télécom ParisTech, in 2001, and the HDR degree from UPMC, in 2007. From January 1998 to October 2000, he was with France Telecom Research and Development. From October 2000 to October 2001, he joined Alcatel Space Industries as a Senior Research Engineer and worked on high data rate modem design for satellites. Since 2001, he has been with Supélec (now CentraleSupélec). He is currently a Full Professor with the CentraleSupélec, Gif-sur-Yvette, France, and a CNRS Researcher. His research interests include information theory, coding theory, and signal processing for telecommunications, with application to the physical layers of satellite, cellular, and vehicular networks.

ALESSANDRO BAZZI (Senior Member, IEEE) received the Laurea degree and the Ph.D. degree in telecommunications from the University of Bologna, in 2002 and 2006, respectively. From 2002 to 2019, he was a Researcher of the National Research Council of Italy (CNR). Since the academic year 2006/2007, he holds courses at the University of Bologna in the area of wireless systems and networks. He is currently a Senior Researcher with the University of Bologna, Italy, and an Associate Member of CNIT/WILAB. His research interests include medium access control and radio resource management of wireless networks. His particular focus has been placed on connected and autonomous vehicles (CAVs), within national and international research projects. He is also part of the ETSI Specialist Task Force on multi-channel operations. He delivered a keynote on CAVs at ICUMT2020, he won the Best Paper Award at ITSC 2017, he participated to several conferences as tutorial instructor or panelist (IARIA MOBILITY 2012, IEEE ISWCS2017, IEEE ComSoc Spring School 2019, and IEEE PIMRC 2019), and he organized Special Sessions or Workshops at IEEE PIMRC 2018 and IEEE PIMRC 2019. He is also in the Editorial Board of *Wireless Communications and Mobile Computing* (Hindawi) and Vehicles (MDPI), and a Chief Editor of *Mobile Information Systems* (Hindawi).